Acknowledgements We acknowledge a generous allotment (of about 3,000 c.p.u. days) of computer time at the supercomputing centre at the Jet Propulsion Laboratory through funding from the NASA Offices of Mission to Planet Earth. Aeronautics and Space Science. Comments from M. Geller improved our paper. The NASA Astrophysics Theory Program supported part of this project.

Competing interests statement The authors declare that they have no competing financial interests.

Correspondence and requests for materials should be addressed to S.J.K. (skenyon@cfa.harvard.edu).

Realization of quantum error correction

J. Chiaverini[1], D. Leibfried[1], T. Schaetz[1]*, M. D. Barrett[1]*, R. B. Blakestad[1], J. Britton[1], W. M. Itano[1], J. D. Jost[1], E. Knill[2], C. Langer[1], R. Ozeri[1] & D. J. Wineland[1]

[1]*Time and Frequency Division,* [2]*Mathematical and Computational Sciences Division, NIST, Boulder, Colorado 80305, USA*

* Present addresses: Max Planck Institut für Quantenoptik, Garching, Germany (T.S.); Physics Department, University of Otago, Dunedin, New Zealand (M.D.B.)

Scalable quantum computation[1] and communication require error control to protect quantum information against unavoidable noise. Quantum error correction[2,3] protects information stored in two-level quantum systems (qubits) by rectifying errors with operations conditioned on the measurement outcomes. Error-correction protocols have been implemented in nuclear magnetic resonance experiments[4–6], but the inherent limitations of this technique[7] prevent its application to quantum information processing. Here we experimentally demonstrate quantum error correction using three beryllium atomic-ion qubits confined to a linear, multi-zone trap. An encoded one-qubit state is protected against spin-flip errors by means of a three-qubit quantum error-correcting code. A primary ion qubit is prepared in an initial state, which is then encoded into an entangled state of three physical qubits (the primary and two ancilla qubits). Errors are induced simultaneously in all qubits at various rates. The encoded state is decoded back to the primary ion one-qubit state, making error information available on the ancilla ions, which are separated from the primary ion and measured. Finally, the primary qubit state is corrected on the basis of the ancillae measurement outcome. We verify error correction by comparing the corrected final state to the uncorrected state and to the initial state. In principle, the approach enables a quantum state to be maintained by means of repeated error correction, an important step towards scalable fault-tolerant quantum computation using trapped ions.

Error-correcting codes that utilize entanglement to rectify unknown errors in qubits are an important ingredient for large-scale quantum information processing[1–3] (QIP). Owing to the fragility of quantum states, the presence of noise during both storage and entangling operations diminishes any gain achieved through the use of QIP without error correction. For example, the realization of long-distance quantum cryptography requires protection from the effects of noise on communication channels[8]. In addition, quantum error correction will be necessary for applications of quantum computing such as efficient factorization of large numbers[1,9]. It is notable that any of an infinite set of qubit errors can be corrected through quantum error correction by means of a finite set of unitary operations conditioned on measurement.

Although there has been extensive theoretical research in the area of quantum error correction, experimental work has been limited to protocol process verifications by means of liquid-state nuclear magnetic resonance. These experiments[4–6] showed an increase in state fidelity after performing the unitary operations of an error-correction protocol, but using techniques known not to scale efficiently with the number of qubits[7]. Furthermore, the ancillae cannot be reset in these experiments, whereas the experiment we describe provides this capability. In principle, the protocol demonstrated here can be repeated with the same qubits as many times as required by a particular quantum algorithm.

We describe the implementation of a quantum error-correcting code (QECC) using three physical qubits, here denoted as the primary qubit and ancillae 1 and 2, to encode and protect one logical qubit from spin-flip errors (a π rotation around the x axis, in this case). Each qubit comprises two hyperfine states of a $^9Be^+$ ion and can be coherently manipulated by means of laser pulses[10,11]. We implement the QECC by (1) preparing the state the primary qubit, (2) encoding this state into the logical state of all three qubits through use of an entangling operation, (3) applying an error rotation (that induces spin-flips upon measurement) to all three qubits, (4) decoding the logical state to the primary qubit, (5) measuring the state of the ancillae, and finally (6) applying correction operations to the primary qubit dependent upon the ancillae measurement outcome. The error correction is performed deterministically in every experiment. The results indicate that such methods, coupled with other recent experimental advances[11–14], may lead to scalable QIP in a system of trapped ions.

In contrast to the standard repetition code[2,3,15], the QECC described and implemented here (see Fig. 1) can not be obtained by application of the superposition principle to a classical error-correction code. It is a stabilizer code[15] with stabilizer group generators $\{ZZX, ZXZ\}$. These generators are tensor products of Pauli operators ($X = \sigma_x, Z = \sigma_z$) operating on the qubits 1, 2 and 3. By calculation of the commutation relations of the generators with various error sets, it can be seen that as an error-detecting code, the QECC presented here detects not only spin-flips on any qubit but also a spin-flip or phase-flip on qubits 2 and 3. As an error-correction code, it will correct a spin-flip on any of the three qubits (the case for this work), but it can instead be used to correct a spin-flip on qubit 1 and a spin-flip or phase-flip on qubit 2 or qubit 3, for example. Another possible implementation can correct a spin-flip on qubit 1 and a phase-flip on either of the other two qubits.

In the experiment, we use $^9Be^+$ ions confined to the axis of a multi-zone linear radio frequency Paul trap[11] similar to that described in ref. 16. The qubits comprise the electronic ground-state hyperfine levels $|F = 1, m_F = -1\rangle$ and $|F = 2, m_F = -2\rangle$ (denoted as $|\uparrow\rangle$ and $|\downarrow\rangle$ respectively, by analogy to the states of a spin-$\frac{1}{2}$ particle). Here F is the total angular momentum and m_F is its projection along the quantization axis. The qubits are entangled with a three-qubit phase gate utilizing the ions' quantized axial vibrational modes[17] (see Methods section and Fig. 2b). Rotations

$$R(\theta,\phi) = \cos\frac{\theta}{2} I - i\sin\frac{\theta}{2}\cos\phi\sigma_x - i\sin\frac{\theta}{2}\sin\phi\sigma_y \qquad (1)$$

are realized with two-photon stimulated-Raman transitions[10,18] implemented by two laser beams having a relative frequency detuning equal to the qubit transition frequency. Here σ_x and σ_y are the usual Pauli operators, I is the identity operator, θ is the rotation angle, and ϕ is the angle of the rotation axis in the x–y plane. Rotations around an axis A by an angle θ will be denoted A_θ, for example, $X_{\pi/2} = R(\pi/2, 0)$, although for rotations around an axis by π we will omit the angle subscript, for example, $X = R(\pi, 0)$.

Measurement is accomplished through projection of the state of each qubit using state-dependent resonance fluorescence (an ion in the $|\downarrow\rangle$ state fluoresces, whereas an ion in the $|\uparrow\rangle$ state does not). The ions can be transported from one zone of the trap to another

through concerted variation of the potentials on segmented control electrodes of the trap, and individual ion detections can be performed separately[11,19].

Ion preparation before each implementation of the QECC protocol consists of Doppler cooling, Raman sideband cooling of all three axial modes of vibration to the ground state, and optical pumping of the ions to the $|\downarrow\downarrow\downarrow\rangle$ state[10,20]. Each experiment also requires the initialization of the primary physical qubit to a state $|\psi_0\rangle_P = \alpha|\uparrow\rangle_P + \beta|\downarrow\rangle_P$ with the ancillae initialized to the state $|\downarrow\downarrow\rangle_A$. This is accomplished by momentarily increasing the spacings between the three ions and then applying a rotation that affects the ions differently owing to their respective positions in the laser beam intensity profile (see Fig. 2a). This operation requires only one laser pulse[10]. The state of the primary qubit is then encoded in the state of all three qubits (see Methods section). In the following discussion we assume perfect entangling operations.

After encoding, we apply an 'error' θ_e, a rotation X_{θ_e}, to all qubits by means of a stimulated-Raman transition with all ions illuminated equally (see equation (1) and top part of Fig. 2a). With respect to later measurement, this error induces a spin-flip on each physical qubit with probability $p(\theta_e) = \sin^2(\theta_e/2)$. The state is then decoded using the inverse of the operation used for encoding. The decoding effects a transformation such that afterwards, the four possible states of the ancillae in the measurement basis (the error syndromes) depend on the type of error that has occurred: the state $|\uparrow\uparrow\rangle_A$ corresponds to no error having occurred, the state $|\uparrow\downarrow\rangle_A$ corresponds to the first ancilla having flipped, the state $|\downarrow\uparrow\rangle_A$ corresponds to the second ancilla having flipped, and the state $|\downarrow\downarrow\rangle_A$ corresponds to the primary qubit having flipped. For at most one qubit flipped, the state of the primary qubit before a correction operation is applied is shown in Table 1.

After the decoding operation, the ions are spatially separated (see Fig. 2c), and a measurement of the state of the ancillae is performed.

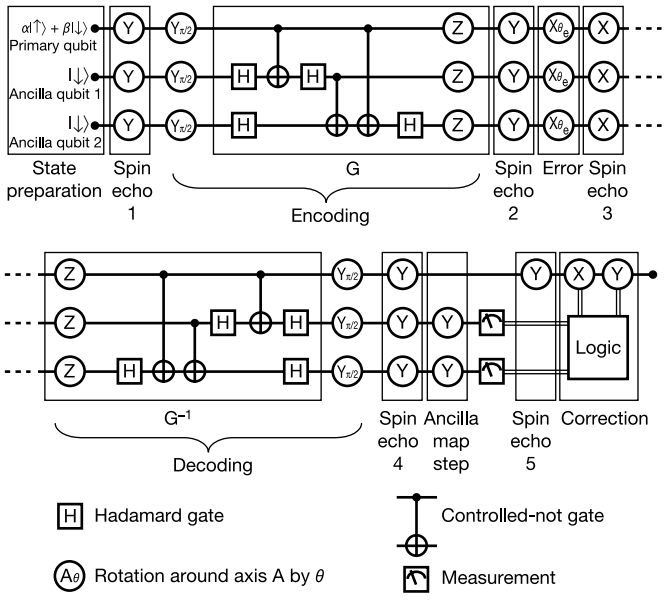

Figure 1 Quantum circuit for the quantum error-correction protocol described and implemented in this work as one would compose it of single-bit rotations, Hadamard gates, and controlled-not gates[15]. Double lines denote classical information. The entangling operation $G(=G^{-1})$ is diagonal in the measurement basis and is defined in the Methods section. The operation of G requires only one collective pulse on all three ions as implemented in this work. The spin echo refocusing operations and ancilla mapping are discussed in the Methods section. For rotations around an axis by π we omit the angle subscript, for example, $X = R(\pi, 0)$ (see equation 1). The Hadamard and controlled-not operations that make up the entangling operation G are equivalent to three controlled-phase rotations between permuted pairs of qubits; these operations could be substituted for the ones shown, depending on the system-dependent entangling gates selected.

The ions are then moved so that only the primary qubit ion is addressed. Depending on the ancillae measurement outcome, a correction operation (X, Y or I, see Table 1) is applied to the primary qubit. This qubit is then analysed to determine the effectiveness of the protocol. After initial cooling and preparation of the state $|\downarrow\downarrow\downarrow\rangle$, each experiment requires approximately 4 ms to perform.

In principle, this QECC works perfectly only when at most one of the three qubits undergoes a spin-flip error. The probability of more than one qubit flipping is given by:

$$P_{2or3}(\theta_e) = p^3(\theta_e) + 3p^2(\theta_e)[1 - p(\theta_e)] \quad (2)$$

Because of this, most input states cannot be corrected to all orders in the error θ_e, though they can be corrected such that an improvement in the fidelity over the uncorrected case is attainable for small errors. The fidelity of the corrected final state (as derivable from the action of the code in Fig. 1) as a function of the error will be:

$$\begin{aligned} F(\theta_e) &= 1 - |\alpha|^2|\beta|^2(2 - 3\cos\theta_e + \cos^3\theta_e) \\ &\approx 1 - \frac{3}{4}|\alpha|^2|\beta|^2\theta_e^4 + O(\theta_e^6) \end{aligned} \quad (3)$$

The infidelity in this case is quadratic in θ_e^2, whereas it is linear in θ_e^2 for the uncorrected state. The fidelity reaches a maximum value of 1 for the cases where $|\alpha|^2|\beta|^2 = 0$. The input states $|\downarrow\rangle_P$ (where $\alpha = 0, |\beta| = 1$) and $|\uparrow\rangle_P$ (where $|\alpha| = 1, \beta = 0$) can therefore be

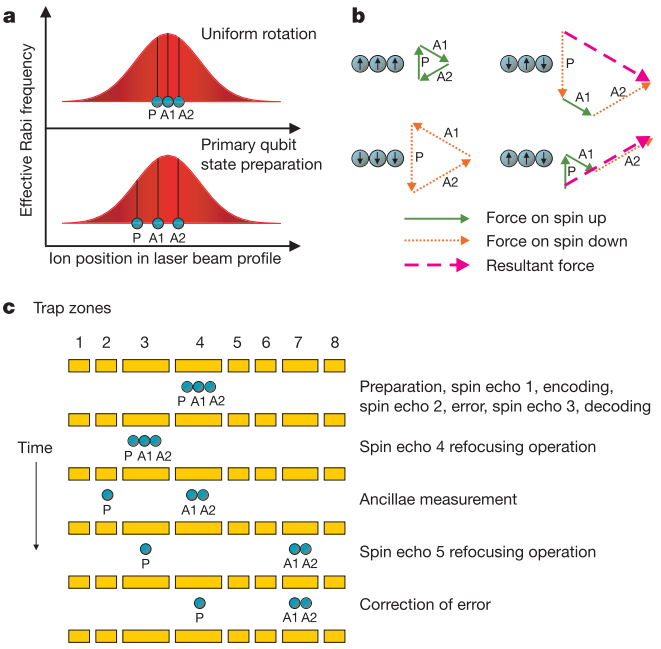

Figure 2 Schematic representation of experimental techniques. **a**, State preparation method. The upper panel depicts ion locations in the laser beam profile for global rotations. In the lower panel, the ions' spacings are increased such that their relative Rabi frequencies for rotations are different (the spacings between the ions relative to the laser beam width are exaggerated in this diagram). By moving the ions such that the primary qubit (labelled P) is at a location of lower radiation intensity, and hence has a lower Rabi frequency than the ancillae A1 and A2 (which are illuminated with equal intensity), a rotation of $2n\pi$ (n an integer; for this experiment $n = 2$) can be performed on the ancillae while any chosen rotation dependent upon the relative Rabi frequencies can be performed on the primary qubit[10]. **b**, Optical-dipole forces (directions indicate relative phase) on ions during the entangling operation G for different internal states. The state-dependent force[18] ($F_\downarrow = -2F_\uparrow$) on each ion leads to accumulation of phase if the centre-of-mass vibrational mode is excited, that is, when the internal states of the ions are different, as in the two diagrams on the right. **c**, Transportation of ions during the error-correction protocol. The three ions' positions are shown as a function of time. Qubit operations are performed on ions in trapping regions 3 and 4, and ion separations are performed in region 3.

Table 1 **Syndromes and corrections for the quantum error-correcting code**

Primary qubit before correction	Error	Ancillary syndrome	Correction operation
$\beta\|\uparrow\rangle_P+\alpha\|\downarrow\rangle_P$	No error	$\|\uparrow\uparrow\rangle_A$	X
$\alpha\|\uparrow\rangle_P+\beta\|\downarrow\rangle_P$	Ancilla 1 flipped	$\|\uparrow\downarrow\rangle_A$	I
$\alpha\|\uparrow\rangle_P+\beta\|\downarrow\rangle_P$	Ancilla 2 flipped	$\|\downarrow\uparrow\rangle_A$	I
$\beta\|\uparrow\rangle_P-\alpha\|\downarrow\rangle_P$	Primary qubit flipped	$\|\downarrow\downarrow\rangle_A$	Y

The first column shows the state of the primary qubit before a correction is applied. The fourth column shows the correction required to recover the primary qubit initial state $|\psi_0\rangle_P=\alpha|\uparrow\rangle_P+\beta|\downarrow\rangle_P$.

corrected to all orders in θ_e for any error X_{θ_e} with this protocol.

To isolate the basic behaviour of the protocol from the technical errors present in the coherent operations required for its implementation, we apply the complete protocol (Fig. 1) with and without application of the error-correction operations and compare the final state fidelities. Figure 3a shows the results for the input state $|\downarrow\rangle_P$. The data are consistent with the theoretical prediction that the state should be corrected for any error X_{θ_e} by this QECC. The curves have non-zero infidelity for zero error angle θ_e owing to infidelity present in the operations of the protocol.

Figure 3b and c shows similar data for the initial states $\sqrt{0.10}|\uparrow\rangle_P-i\sqrt{0.90}|\downarrow\rangle_P$ and $\sqrt{0.22}|\uparrow\rangle_P-i\sqrt{0.78}|\downarrow\rangle_P$ respectively. From equation (3), it can be seen that as the input state gets closer to the equator of the Bloch sphere ($|\alpha|\approx|\beta|$), the QECC is expected to perform worse for larger errors. However, the infidelity of the corrected state should grow only quadratically in θ_e^2 for small errors, as opposed to a linear growth for the uncorrected state. This behaviour can be observed in the data, which in all cases show an improvement over the uncorrected state. Data for a full range of input states are not presented, as input states with larger values of $|\alpha|$ required larger ion spacings and lower axial confining potentials than were practical during preparation of the primary qubit state; these configurations were temporally unstable in the current apparatus. It should be noted, however, that these experimental limitations to state preparation do not affect the QECC protocol.

We also plot the observed rate of the ancillary syndromes for a particular input state in Fig. 3d to verify that our QECC protocol is correctly detecting errors. The rate $\Gamma(|\uparrow\uparrow\rangle_A)$ of the syndrome corresponding to no error and the sum of the rates $\Gamma(|\uparrow\downarrow\rangle_A)+\Gamma(|\downarrow\uparrow\rangle_A)+\Gamma(|\downarrow\downarrow\rangle_A)$ of the syndromes corresponding to one error are plotted separately. The rates of the syndromes vary in the predicted manner for increasing error, up to an offset due to imperfections in the operations that make up the protocol.

Although an improvement in fidelity over an uncorrected encoded qubit was observed, the QECC protocol as implemented here induced more infidelity for small errors than would be acquired if an unencoded qubit had been initialized and then been subject only to the applied error. It should be noted, however, that for errors

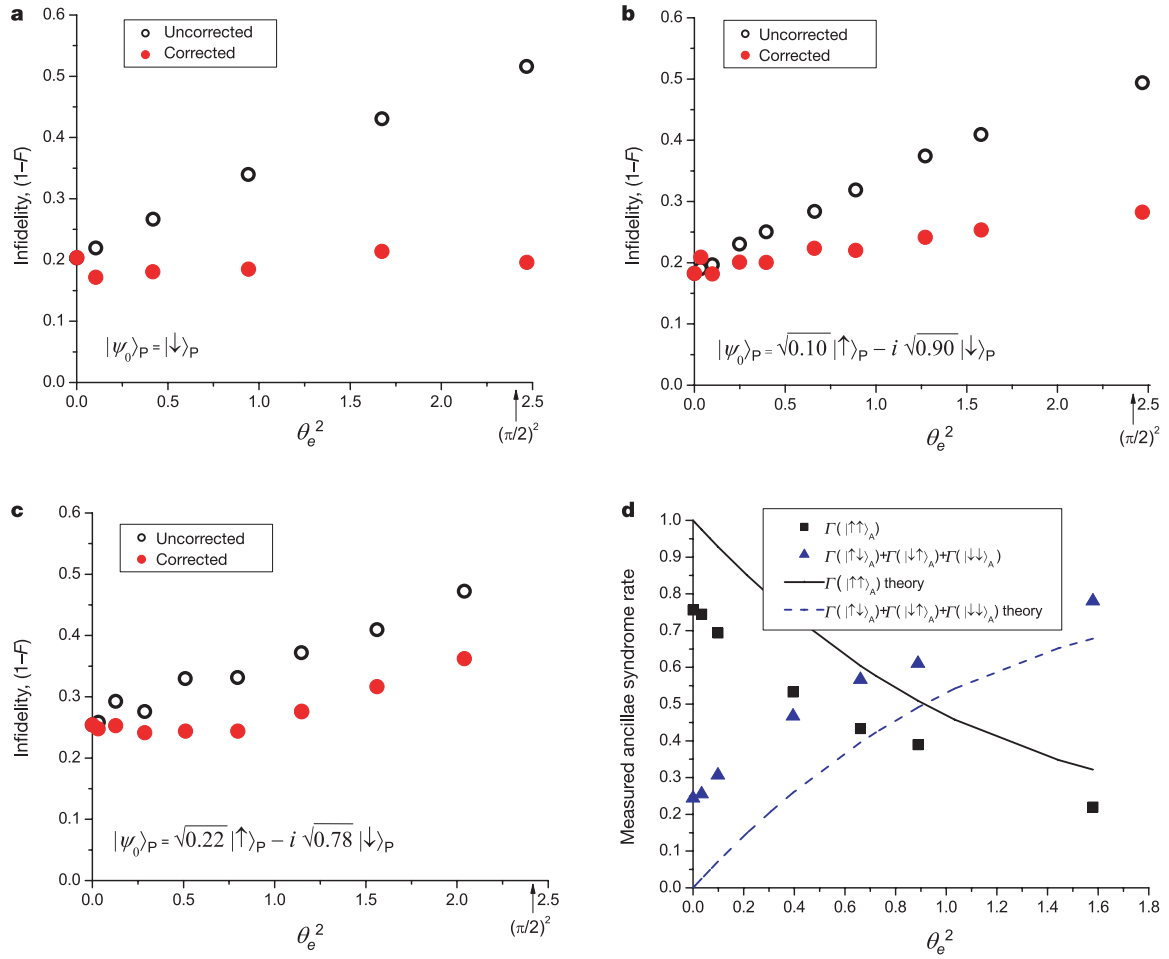

Figure 3 Results of quantum error correction protocol. Recovered state infidelity plotted versus the square of the applied error for corrected and uncorrected cases for three initial states (**a**–**c**) and rate of syndrome measurements of ancillae (**d**). One-standard-deviation errors are approximately the size of the symbols. **a**, The initial state is $|\psi_0\rangle_P=|\downarrow\rangle_P$. **b**, The initial state is $|\psi_0\rangle_P=\sqrt{0.10}|\uparrow\rangle_P-i\sqrt{0.90}|\downarrow\rangle_P$. **c**, The initial state is $|\psi_0\rangle_P=\sqrt{0.22}|\uparrow\rangle_P-i\sqrt{0.78}|\downarrow\rangle_P$. **d**, Rate of syndrome measurements of ancillae versus square of error angle. The rate $\Gamma(m)$ is the measured probability of obtaining the measurement outcome m. The data are off-set from the theoretical curves because of imperfect gate operations. The initial state is $|\psi_0\rangle_P=\sqrt{0.10}|\uparrow\rangle_P-i\sqrt{0.90}|\downarrow\rangle_P$ for these data.

larger than $\theta_e \approx 1$ radian, the corrected state had higher fidelity than an unencoded qubit undergoing only an applied error for all states investigated, and the logical state was genuinely protected with this protocol. The degradation observed during the execution of the QECC is due in large part to the fidelity of the encoding and decoding gates (~90%), and all operations must be improved to achieve fault-tolerance. In spite of these technical difficulties, the current experiment shows the viability of the error-correction protocol and demonstrates the feasibility of quantum error correction in a scalable system in which the ancillae can be reset. With improvements in fidelity, the execution of the QECC can be made a useful part of more complex quantum algorithms. □

Methods

Encoding and decoding

To encode the logical state with the QECC, we implement a three-ion entangling operation, an extension of those described previously[12,17]:

$$G(s_1,s_2,s_3) = G^{-1}(s_1,s_2,s_3) = \begin{cases} 1 & \text{if } s_1 = s_2 = s_3 \\ -1 & \text{otherwise} \end{cases} \quad (4)$$

Here $s_i \in \{\uparrow, \downarrow\}$ is the spin state of the ith ion. This operation is diagonal in the measurement basis and is equivalent to that depicted by G in Fig. 1, as can be verified by explicit calculation. A 'walking wave' polarization interference pattern is set up at the ions' location using two perpendicular beams of radiation whose wavevector difference is parallel to the trap axis and whose difference frequency is detuned by a small amount δ ($\approx 2\pi \times 70$ kHz) from the frequency ω_{COM} ($= 2\pi \times 3.7$ MHz) of the centre-of-mass (COM) axial vibrational mode in the trap[17,18]. The inter-ion spacing is adjusted relative to the beams' interference pattern so that if the phase of the resulting oscillating optical-dipole force at frequency $\omega_{COM} - \delta$ at the primary ion is ϕ_P, the phases at the ancillae ions are $\phi_{A1} = \phi_P + \frac{2\pi}{3}$ and $\phi_{A2} = \phi_P + \frac{4\pi}{3}$. The axial COM mode will be (off-resonantly) excited only if there is a net force on the ions, which is the case if the ions are in different internal states, that is, for all states except $|\uparrow\uparrow\uparrow\rangle$ and $|\downarrow\downarrow\downarrow\rangle$ (see Fig. 2b). As the vibrational mode is excited, the ions move along a closed path in phase space (if the radiation is applied for a time equal to $2\pi/\delta$), and the states acquire a phase proportional to the phase-space area enclosed by this path. All states except those for which $s_1 = s_2 = s_3$ acquire the same phase (adjusted to be π), as the magnitude of the net force on the ions is equal and non-zero. The application of a global rotation $Y_{\pi/2}$ followed by this entangling gate implements the 'Encoding' section of Fig. 1. The application of an error is followed by a re-application of the three-ion entangling gate G and a final global rotation $Y_{\pi/2}$; this implements the 'Decoding' section of Fig. 1.

Refocusing and auxiliary operations

To simplify the syndrome determination when the ancillae are measured together, the protocol is designed such that an X operation is required to return the protected qubit to its initial state if no error has occurred, while no operation (the identity) is required if either one of the ancillae is flipped, and a Y operation is required if the primary bit is flipped. The protocol was implemented in this fashion through the tailoring of the phases of two spin echo refocusing pulses[11,16,17] that are required between encoding and decoding (spin echoes 2 and 3 in Fig. 1) to counteract qubit dephasing caused by fluctuations in the local magnetic field from experiment to experiment. The time required for ion transportation in the trap necessitates additional spin-echo operations after decoding and before correction (spin echoes 4 and 5). To reduce experimental measurement uncertainty, an ancilla mapping step is performed to associate the outcome that is expected most often (no error) with the ancillae state $|\uparrow\uparrow\rangle_A$, the state most easily distinguishable from the others when the ancillae are measured together.

After the correction operation is applied to the primary qubit, we apply a rotation X_{θ_F} to this qubit before measurement to characterize the effectiveness of the protocol. The angle θ_F is varied over many experiments such that we produce a sinusoidal trace of the probability of measuring the primary qubit to be in the state $|\downarrow\rangle_P$ as it is rotated around the Bloch-sphere axis around which the error was applied. This allows a fit to a sinusoidal curve and hence precise measurement of the final state fidelity of the primary qubit.

Received 30 August; accepted 1 October 2004; doi:10.1038/nature03074.

1. Preskill, J. Reliable quantum computers. *Proc. R. Soc. Lond. A* **454,** 385–410 (1998).
2. Calderbank, A. R. & Shor, P. W. Good quantum error-correcting codes exist. *Phys. Rev. A* **54,** 1098–1105 (1996).
3. Steane, A. Multiple particle interference and quantum error correction. *Proc. R. Soc. Lond. A* **452,** 2551–2577 (1996).
4. Cory, D. G. *et al.* Experimental quantum error correction. *Phys. Rev. Lett.* **81,** 2152–2155 (1998).
5. Leung, D. *et al.* Experimental realization of a two-bit phase damping quantum code. *Phys. Rev. A* **60,** 1924–1943 (1999).
6. Knill, E., Laflamme, R., Martinez, R. & Negrevergne, C. Benchmarking quantum computers: The five-qubit error correcting code. *Phys. Rev. Lett.* **86,** 5811–5814 (2001).
7. Cory, D. G. *et al.* NMR based quantum information processing: Achievements and prospects. *Fortschr. Phys.* **48,** 875–907 (2000).
8. Lo, H.-K. & Chau, H. F. Unconditional security of quantum key distribution over arbitrarily long distances. *Science* **283,** 2050–2056 (1999).
9. Shor, P. W. *Proc. 35th Annual Symp. on Foundations of Computer Science* (ed. Goldwasser, S.) 124 (IEEE Computer Society Press, Los Alamitos, California, 1994).
10. Wineland, D. J. *et al.* Experimental issues in coherent quantum-state manipulation of trapped atomic ions. *J. Res. Natl Inst. Stand. Technol.* **103** (3), 259–328 (1998).
11. Barrett, M. D. *et al.* Deterministic quantum teleportation of atomic qubits. *Nature* **429,** 737–739 (2004).
12. Leibfried, D. *et al.* Toward Heisenberg-limited spectroscopy with multiparticle entangled states. *Science* **304,** 1476–1478 (2004).
13. Riebe, M. *et al.* Deterministic quantum teleportation with atoms. *Nature* **429,** 734–737 (2004).
14. Blinov, B. B., Moehring, D. L., Duan, L.-M. & Monroe, C. Observation of entanglement between a single trapped atom and a single photon. *Nature* **428,** 153–157 (2004).
15. Nielsen, M. A. & Chuang, I. L. *Quantum Computation and Quantum Information* (Cambridge Univ. Press, Cambridge, UK, 2000).
16. Rowe, M. A. *et al.* Transport of quantum states and separation of ions in a dual rf ion trap. *Quant. Inf. Comput.* **2,** 257–271 (2002).
17. Leibfried, D. *et al.* Experimental demonstration of a robust, high-fidelity geometric two ion-qubit phase gate. *Nature* **422,** 412–415 (2003).
18. Wineland, D. J. *et al.* Quantum information processing with trapped ions. *Phil. Trans. R. Soc. Lond. A* **361,** 1349–1361 (2003).
19. Schaetz, T. *et al.* Quantum dense coding with atomic qubits. *Phys. Rev. Lett.* **93,** 040505 (2004).
20. King, B. E. *et al.* Cooling the collective motion of trapped ions to initialize a quantum register. *Phys. Rev. Lett.* **81,** 1525–1528 (1998).

Acknowledgements We thank T. Rosenband and D. Rosenberg for comments on the manuscript. This work was supported by the US National Security Agency (NSA) and the Advanced Research and Development Activity (ARDA). This manuscript is a publication of NIST.

Competing interests statement The authors declare that they have no competing financial interests.

Correspondence and requests for materials should be addressed to J.C. (john.chiaverini@boulder.nist.gov).

Nonlinear optics in the extreme ultraviolet

Taro Sekikawa, Atsushi Kosuge, Teruto Kanai & Shuntaro Watanabe

Institute for Solid State Physics, University of Tokyo, 5-1-5 Kashiwanoha, Kashiwa 277-8581, Japan

Nonlinear responses to an optical field are universal in nature but have been difficult to observe in the extreme ultraviolet (XUV) and soft X-ray regions owing to a lack of coherent intense light sources. High harmonic generation is a well-known nonlinear optical phenomenon[1,2] and is now drawing much attention in attosecond pulse generation[3–6]. For the application of high harmonics to nonlinear optics in the XUV and soft X-ray regime, optical pulses should have both large pulse energy and short pulse duration to achieve a high optical electric field. Here we show the generation of intense isolated pulses from a single harmonic (photon energy 27.9 eV) by using a sub-10-femtosecond blue laser pulse, producing a large dipole moment at the relatively low (ninth) harmonic order nonadiabatically[7,8]. The XUV pulses with pulse durations of 950 attoseconds and 1.3 femtoseconds were characterized by an autocorrelation technique, based on two-photon above-threshold ionization[9] of helium atoms. Because of the small cross-section for above-threshold ionization[10], such an autocorrelation measurement of XUV pulses with photon energy larger than the ionization energy of helium has not hitherto been demonstrated[6,11–13]. The technique can be extended to the characterization of higher harmonics at shorter wavelengths.

The two-photon above-threshold ionization (ATI) of helium atoms is a successive absorption of an additional photon beyond the one required for ionization of helium atoms. The cross-section of two-photon ATI is an order of magnitude smaller than conven-